

EFFECT OF ZnS BUFFER LAYER ON PERFORMANCE OF CIGS SOLAR CELL

●Laid Abdelali^a, Hamza Abid^a, ●Ikram Zidani^a, ●Aissa Meksi^b, ●Abdellah Bouguenna^{c*},
Zaid Bendaoudi^d

^aApplied Material Laboratory, University Djillali Liabes of Sidi Bel Abbes, Algeria

^bElectrical Engineering Department University of Sciences and Technology of Oran, Algeria B.P 1505, El Mnaouer, Oran, Algeria

^cElectrical Engineering Laboratory of Oran, Department of Electronics, Faculty of Electrical Engineering, University of Sciences & Technology of Oran (MB-USTO), 31000, Oran, Algeria

^dDepartment of Electrotechnical & Automatic Engineering, University of Relizane, Algeria

*Corresponding Author e-mail: abdellah.bouguenna@univ-usto.dz

Received July 9, 2024; revised September 18, 2024; accepted September 25, 2024

Cu(In,Ga)Se₂ (CIGS)-based thin-film solar cells are currently among the most efficient. Zinc sulfide (ZnS) is the best buffer layer used in CIGS-based solar cells because it is non-toxic and has a wide band gap. In this study, we present a simulation of a CIGS solar cell with a ZnS buffer layer, carried out using the Silvaco-Atlas simulator. We attained an efficiency of 24.13%, short-circuit current of 37.81 mA/cm², an open circuit voltage of 740 mV and a fill factor of 78.78% at a bandgap around 1.41 eV, corresponding to an x ratio of 0.5. The photovoltaic performance of the ZnS/CIGS solar cell is improved by optimizing the effects of layer parameters such as thickness, acceptor and donor densities of the CIGS absorber and ZnS buffer layers. For a 0.035 μm thick ZnS acceptor with a density of 6 × 10¹⁷ cm⁻³ and a 3 μm thick CIGS donor with a density of 10¹⁸ cm⁻³, a maximum efficiency improved to 27.22%.

Keywords: Buffer layer (ZnS); CIGS; Solar cell; Optimization; Silvaco-Atlas

PACS: 84.60.Jt; 78.20.Bh; 89.30.Cc; 42.60.Lh.

1. INTRODUCTION

Due to its lower production costs, higher conversion efficiency and enhanced stability, the thin-film solar cell based on the CIGS compound semiconductor has recently grown in popularity. In the visible solar spectrum, the CIGS compound semiconductor offers captivating features, such as a directly controllable bandgap from (1.0 to 1.7 eV) to maximize irradiance, and an absorption factor of 10⁶ cm⁻¹. CIGS and CdS solar cells are the most popular thin-film photovoltaic technology, with an energy conversion efficiency of 22.6%. When the 2.4 eV bandgap is unsuitable for solar cells, the CdS buffer layer shows optical absorption losses, particularly in the short-wave range [3, 4]. In addition, because of the hazardous cadmium (Cd) waste produced during deposition, the CdS buffer layer can pose a risk to human health and the environment. Given these factors, the CIGS absorption layer is compatible with other wide-bandgap buffer layers. Zinc sulfide (ZnS) prepared using chemical bath deposition (CBD) offers an attractive alternative to CdS in collaboration with CIGS absorbers [8, 9] due to its wide bandgap of around 3.68 eV and its non-toxicity to the environment. Cell efficiency is enhanced by ZnS/CIGS, Zn_{1-x}Sn_xO_y and CIGS, In_xS_y/CIGS, with rates of 21.0% [5], 18.2% [6] and 18.1% [7] respectively.

The energy of zinc sulfide (ZnS) is much higher than that of CdS in the bandgap. The ZnS buffer layer used in CIGS solar cells improves current generation at shorter wavelengths. CIGS solar cells with a ZnS buffer layer perform almost identically to CdS/CIGS solar cells [10-11]. The use of solar cell simulation has become an essential tool for studying their operation and improving the design of high-performance solar cells. In this research, we perform a simulation of both CIGS and ZnO/ZnS/CIGS solar cells to evaluate their performance [12, 14, 15, 16], where ZnS/CIGS solar cells are more promising than CdS/CIGS solar cells [2, 17].

The main parameters of ZnS/CIGS cells have been identified by several numerical studies, such as thickness, bandgap, gradient of the CIGS absorber layer and thickness of the ZnS buffer layer [17, 18, 19, and 20].

In this article, we examine ZnS/CIGS solar cells using simulation studies. Numerical analysis of CIGS solar cells is presented using the Silvaco-Atlas simulator (AM1.5 G, 100 mW/cm², 300 K) to determine basic parameters (J_{sc}, V_{oc}, FF and η). We use ZnS as a buffer layer to study the performance of CIGS solar cells, and have simulated our structure to study photovoltaic characteristics. We compared the performance of a CIGS solar cell with a ZnS buffer layer with other works [21, 22]. The consequences of the thickness of the absorber layer, the temperature and the impact of the CIGS absorber layer in the band gap. The efficiency of this solar cell is 24.13%, thanks to the use of ZnS and CIGS.

2. Modeling and simulation parameters

2.1. Structure simulated

Figure 1 shows schematically the structure of the CIGS solar cell examined in this study. It consists of a single-junction solar cell based on a CIGS that is both optically and electrically connected, with a layer of ZnO serving as a transparent coating. Figure 1 shows the doping concentrations and thicknesses of the various layers that make up the

simulated structure. The CIGS consists of a transparent n-type ZnO contact layer, an n-type ZnS buffer layer and a p-type CIGS absorber layer. Finally, a layer of Molybdenum (Mo) on a glass substrate is often used as a back contact.

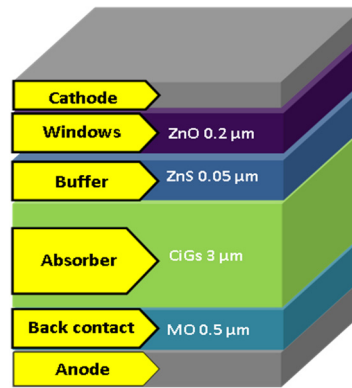


Figure 1. Structure of CIGS solar cell

2.2. Physical models

The Silvaco Atlas simulation software was used in this study. Atlas is a two- and three-dimensional physics-based device simulator that enables us to numerically solve the Poisson's equation coupled to the continuity equations for electrons and holes under stationary conditions. Newton's method is the default method selected for solving the basic semi-conductor equations in the software [23]. The various basic parameters used in this work include band gaps E_g , relative permittivity ϵ_r , electronic affinity χ_e , charge carrier mobility in the conduction band μ_n , charge carrier mobility in the valence band μ_p , effective density of states in the conduction band N_C , the effective density of states in the valence band N_V , the Gaussian defect density N_{GA} , N_{GD} , the maximum energy position E_{GA} , E_{GD} , the standard energy deviation W_{GA} , W_{GD} , the electron capture cross section σ_n , the hole capture cross section σ_p , and the surface recombination velocity parameters of electrons S_n and holes S_p .

Table 1 [1, 13, 22, 24] shows the parameters for each layer of the solar cell, which serve as input data for the Atlas-Silvaco numerical simulation.

Table 1. Material parameters used in the simulation.

Layer properties	ZnO	ZnS	CIGS
E_g (eV)	3.3	3.68	Varied
ϵ_r	4.1	4.5	4.8
χ_e (eV)	9	8.32	13.9
μ_n (cm^2/Vs)	100	250	100
μ_p (cm^2/Vs)	25	40	25
N_c (cm^{-3})	2.2×10^{18}	1.5×10^{18}	2.2×10^{18}
N_v (cm^{-3})	1.8×10^{19}	1.8×10^{19}	1.8×10^{19}
Gaussian defect states			
N_{DG}, N_{VG} ($1/cm^3$)	$D : 10^{17}$	$A : 10^{15}$	$D : 10^{15}$
E_A, E_D (eV)	Mid gap	Mid gap	Mid gap
W_G (eV)	0.1	0.1	0.1
σ_e (cm^2)	10^{-12}	10^{-17}	10^{-13}
σ_h (cm^2)	10^{-15}	10^{-13}	10^{-15}

In this simulation, we use the illumination conditions of the AM1.5 G solar spectrum at one sun, with an incident power density of 100 mW/cm^2 and an ambient temperature of 300°K . The bandgap of $\text{CuIn}_{1-x}\text{Ga}_x\text{Se}_2$ was calculated using the empirical expression:

$$E_g[\text{eV}] = 1.010 + 0.626 \cdot x - 0.167x(1 - x) \quad (1)$$

Where E_g varies from 1.0692 eV to 1.7609 eV for $x=0$ (CIS) and $x=1$ (CGS), respectively [25].

Ga composition was set at 0.30, corresponding to a bandgap energy of 1.27 eV.

ATLAS offers a variety of models that can be used to simulate devices. We have used the Density of States (DOS) model to represent the defect density in CIGS and ZnS layers. The data provide two deep-level bands, modeled using a Gaussian distribution.

$$g_{GA}(E) = N_{GA} \exp \left[- \left[\frac{E_{GA} - E}{W_{GA}} \right]^2 \right] \tag{2}$$

$$g_{GD}(E) = N_{GD} \exp \left[- \left[\frac{E - E_{GD}}{W_{GD}} \right]^2 \right] \tag{3}$$

In this situation, E corresponds to the fault energy, while the indices (G, A, D) correspond to Gaussian fault states, acceptors and donors respectively. Density states are defined by their effective density N_{GA} or N_{GD} , their standard energy gap W_{GA} or W_{GD} , and their maximum energy position E_{GA} or E_{GD} [23].

In the standard model, the Gaussian defect distribution is used to describe the defect states of semiconductor materials with defects. Shockley-Read-Hall recombination is modeled as follows:

$$R_{SRH} = \frac{pn - n_i^2}{\tau_p \left(n + n_i \exp \frac{E_i - E_T}{KTL} \right) + \tau_n \left(p + n_i \exp \frac{-(E_i - E_T)}{KTL} \right)} \tag{4}$$

$$\tau_n = \frac{1}{\sigma_n v_{th} N_t} \text{ and } \tau_p = \frac{1}{\sigma_p v_{th} N_t}$$

Where τ_n and τ_p are the electrons and holes lifetime parameters (TAUN0 and TAUP0 in Silvaco Atlas), σ_n and σ_p are the capture cross sections for electrons and holes, respectively, v_{th} is the thermal velocity, and N_t is the trap density by volume. n_i is a spatially varying intrinsic concentration level, E_i is the intrinsic Fermi energy level, E_T is the trap energy level, ($E_i - E_T$ is ETRAP in Silvaco Atlas), and T_L is the lattice temperature in Kelvin [23,26].

A general expression for surface recombination is:

$$R_{surf} = \frac{pn - n_i^2}{\tau_p^{eff} \left(n + n_i \exp \frac{E_i - E_T}{KTL} \right) + \tau_n^{eff} \left(p + n_i \exp \frac{-(E_i - E_T)}{KTL} \right)} \tag{5}$$

$$\frac{1}{\tau_n^{eff}} = \frac{1}{\tau_n^i} + \frac{d_i}{A_i} S.N \text{ and } \frac{1}{\tau_p^{eff}} = \frac{1}{\tau_p^i} + \frac{d_i}{A_i} S.P$$

where τ_p^i and τ_n^i are the volume lifetimes calculated at node i along the interface, which may also be a function of impurity concentration. Parameters d_i and A_i are the interface length and area for node i. Parameters S.N and S.P are the recombination velocities for electrons and holes respectively [27].

3. Simulation Results and Discussion

3.1. Optimal CIGS absorbing layer bandgap

The electrical parameters of the CIGS cell were calculated for different values of the bandgap of the CIGS absorber layer to determine the optimum efficiency-enhancing bandgap. We set the thickness of the CIGS absorber layer at 3 μm and varied the bandgap by changing the X ratio from 0 to 1.

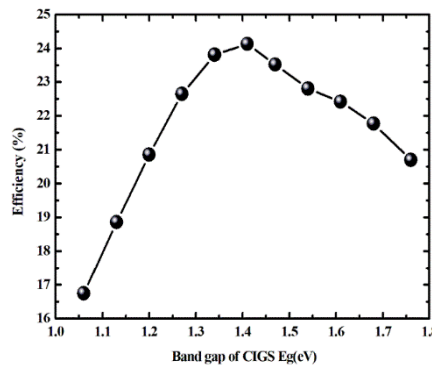


Figure 2. The variation band gap energy of CIGS as function of efficiency

The characteristics of the CIGS cell for different band gaps as a function of efficiency are shown in Figure 2. It can be seen that increasing the band gap of the CIGS absorber layer, and hence increasing the x-ratio, leads to a proportional increase in efficiency up to a value of 1.4 and then the efficiency starts to decrease, the efficiency increase starts from

16.75% to 24.13%. The excellent efficiency obtained for the CIGS solar cell is 24.13%. The optimum efficiency of the CIGS cell was achieved when the optical bandgap was around 1.41 eV, corresponding to an x ratio of 0.5.

3.2. Influence of absorber layer thickness

The CIGS solar cell structure, obtained using Silvaco-Atlas, is shown in Figure 3.

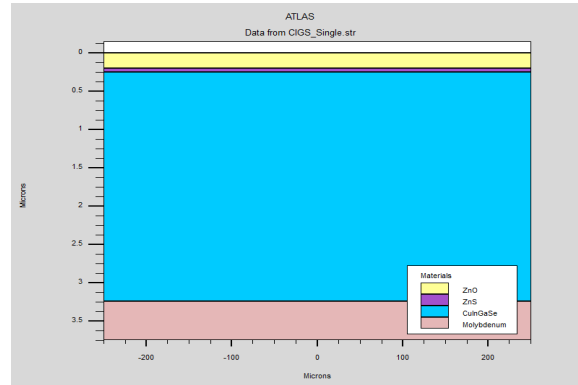


Figure 3. Silvaco-Atlas structure file of the CIGS solar cell

In this section of the simulation, we first opted for a CIGS layer thickness of 2 μm , then adjusted the thickness of the zinc sulfide (ZnS) buffer layer from 0.1 μm to 0.03 μm .

We observed that the efficiency increases and then decreases with increasing ZnS buffer layer thickness. We also found that the high efficiency of CIGS thin-film solar cells decreases as the thickness of the zinc sulfide buffer layer increases (from 22.45% for 0.035 μm to 20.91% for 0.1 μm). As is obvious, the performance of all solar cells decreases as the buffer layer thickness increases, with the exception of open-circuit voltage, which remains constant. Even if some absorption losses in solar cells are caused by the ZnS buffer layer or emitter thickness, this may explain the profile of this result. The ZnS layer has a thickness ranging from 10 nm to 30 nm, while the CIGS layer varies from 1 μm to 4 μm . Figures 4, 5, 6 and 7 shows the impact of ZnS layer thickness on the performance of CIGS-based solar cells. The short-circuit current density increases from 30.69 to 35.70 mA/cm^2 as the thickness of the ZnS buffer layer increases from 10 to 35 nm.

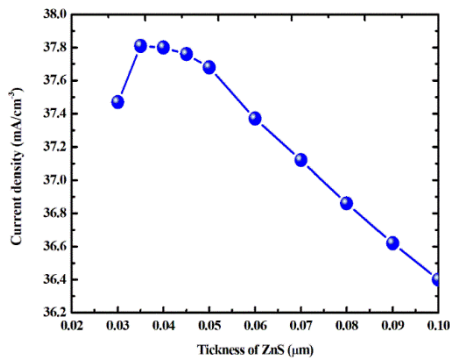


Figure 4. Effect of ZnS buffer layer thickness on the current density of the CIGS solar cells

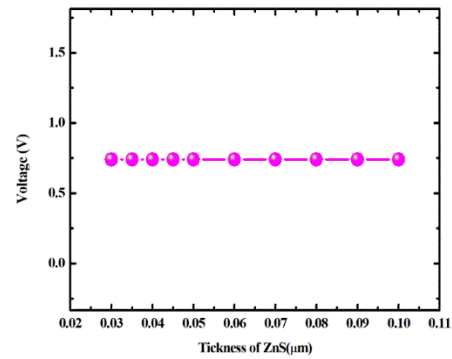


Figure 5. Effect of ZnS buffer layer thickness on the voltage of the CIGS solar cells

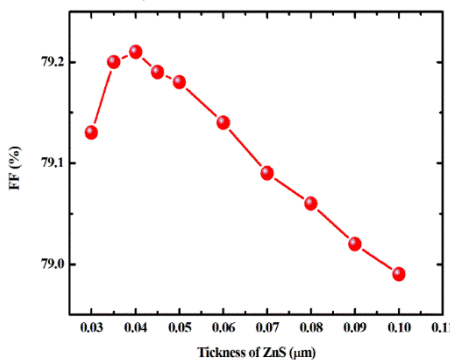


Figure 6. Effect of ZnS buffer layer thickness on the factor form of the CIGS solar cells

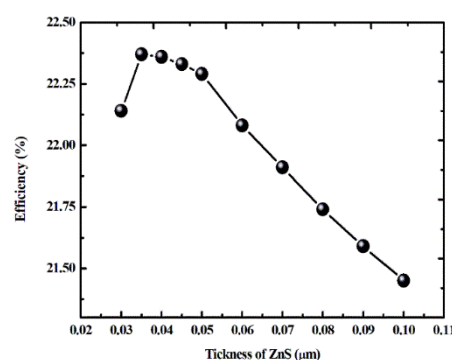


Figure 7. Effect of ZnS buffer layer thickness on the efficiency of the CIGS solar cells

The increase leads to a rise in the solar cell's conversion rate. In physical terms, a very thin absorber layer indicates that the back contact and the depletion zone are very close, which favors electron capture by this contact. This form of recombination process affects cell performance, as it has an impact on conversion efficiency.

3.3. Effect of temperature on CIGS solar cells using ZnS as buffer layer

One of the most crucial parameter optimizations for thin-film solar cells is operating temperature, which plays an important role in assessing thin-film performance.

We are studying the influence of temperature on CIGS-based solar cells, using ZnS as a buffer layer. As we can see, the performance of thin-film solar cells decreases with increasing operating temperature. The same variation in performance properties with increasing operating temperature. This indicates that ZnS could be a good alternative material for use in photovoltaic applications.

Figure 8 shows the influence of operating temperature on CIGS-based solar cells using ZnS as a buffer layer.

Extracted from the various (J - V) characteristics shown in Figure 9, the electrical parameters of the CIGS cell are summarized in Table 2 and compared with the published data [21, 22], our simulated results represent higher efficiency than them.

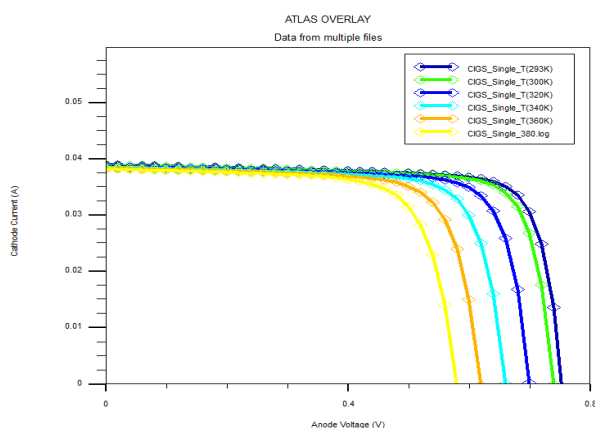


Figure 8. Effect of the Temperature on performance of solar cells, using ZnS as Buffer layer

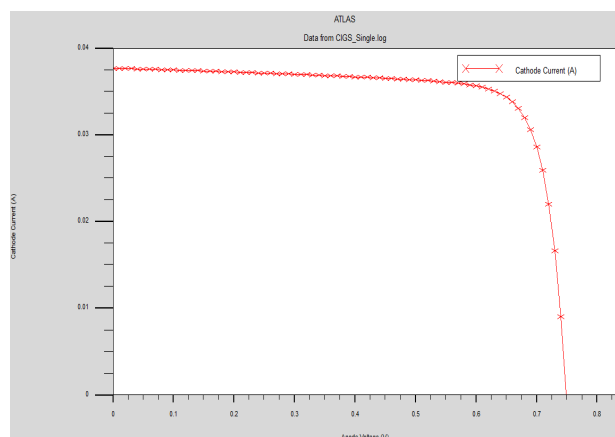


Figure 9. Simulation J - V characteristics of the ZnS/CIGS solar cell

Table 2. Comparison between our model and other works

	Voc (mv)	Jsc (mA/ cm ²)	FF (%)	η (%)
Our Simulation ZnS/CIGS (Eg=1.2 eV)	0.74	37.68	79.18	22.29
Simulation of [21] ZnS/CIGS (Eg=1.2 eV)	0.71	37.96	81.24	22.16
Our Simulation ZnS/CIGS (Eg=1.41 eV, x=0.5)	0.74	37.81	78.78	24.13
Simulation of [22] ZnS/CIGS (Eg=1.41 eV, x=0.5)	0.804	35.66	82.14	23.54

It is conceivable that the simulated data will serve as a starting point for modeling the effect of absorber layer thickness, absorber layer bandgap and the use of ZnS as a buffer layer on solar cell performance in our work.

In this study, we aim to obtain the highest current values for the CIGS cell and find an optimum matching efficiency for the simulated structure.

4. CONCLUSION

In this work, we have presented and discussed the results of a numerical simulation study of the electrical characteristics of a CIGS-based thin-film hetero-junction solar cell. Of the electrical characteristics of a CIGS-based thin-film hetero-junction solar cell, generated by the Silvaco Atlas-2D simulation software.

We studied the electrical stimulation of the CIGS cell with the ZnS cell, proving that the ZnS cell is better than the other cells. Then we studied the impact of two layers in ZnS (buffer layer) and CIGS (absorber layer) with the aim of designing an optimal ZnO/ZnS/CIGS hetero-junction structure that gives the best electrical performance. We conclude from this study that the best doping for the ZnS layer is concentration $6 \times 10^{17} \text{ cm}^{-3}$ with a thin thickness of 35 nm and the best doping for the CIGS layer of concentration $1 \times 10^{18} \text{ cm}^{-3}$ with a thickness of 3 μm to obtain the optimum electrical efficiency of 27.22%.

Declaration of competing interests: The authors declare that they have no financial interests or personal relationships that may have influenced the work presented in this article.

Acknowledgments

This study is supported by the applied materials laboratory, university of Sidi Bel Abbas, Algeria.

ORCID

Laid Abdelali, <https://orcid.org/0009-0009-9173-3835>;
 Ikram Zidani, <https://orcid.org/0009-0003-8900-5261>
 Aissa Meksi, <https://orcid.org/0009-0007-1698-5069>;
 Abdellah Bouguenna, <https://orcid.org/0000-0003-3492-5418>

REFERENCES

- [1] H. Heriche, Z. Rouabah, and N. Bouarissa, *Int. J. Hydrogen Energy*, **42**(15), 9524-9532 (2017). <https://doi.org/10.1016/j.ijhydeng.2017.02.099>
- [2] P. Jackson, R. Wuerz, D. Hariskos, E. Lotter, W. Witte, and M. Powalla, *Rapid Research Letters*, **10**(8), 583 (2016). <https://doi.org/10.1002/psrr.201600199>
- [3] D. Hariskos, S. Spiering, and M. Powalla, *Thin Solid Films*, **480**, 99-109 (2005). <https://doi.org/10.1016/j.tsf.2004.11.118>
- [4] M.A. Green, Y. Hishikawa, E.D. Dunlop, D.H. Levi, J. Hohl- Ebinger, M. Yoshita, and W.Y. Ho-Baillie Anita, Solar cell efficiency tables (Version 53), *Prog. Photovolt Res. Appl.* **27**, 3–12 (2019). <https://doi.org/10.1002/ppp.3102>
- [5] T. M. Friedlmeier, P. Jackson, A. Bauer, D. Hariskos, O. Kiowski, R. Wuerz, and M. Powalla, *IEEE Journal of Photovoltaics* **5**(5), 1487-1491 (2015). <https://doi.org/10.1109/JPHOTOV.2458039>
- [6] S. Spiering, A. Nowitzki, F. Kessler, M. Igalson, and H. A. Maksoud, *Solar Energy Materials and Solar Cells*, **144**, 544-550 (2016), <https://doi.org/10.1016/j.solmat.2015.09.038>
- [7] T. Törndahl, A. Hultqvist, C. Platzer-Björkman, and M. Edoff, in: *Proceedings Volume 7603, Oxide-based Materials and Devices International Society for Optics and Photonics*, (San Francisco, California, United States, 2010), p. 76030D <https://doi.org/10.1117/12.846351>
- [8] M.A. Olopade, O.O. Oyebola, and B.S. Adeleke, *Adv. Appl. Sci. Res.* **3**, 3396 (2012).
- [9] T. Kobayashi, T. Kumazawa, Z.J.L. Kao, and T. Nakada, *Energy Mater. Sol. Cells*, **119**, 129 (2013). <https://doi.org/10.1016/j.solmat.2013.05.052>
- [10] M. Fedawy, S.M. Ali, and T. Abdolkader, *Journal of Advanced Research in Materials Science*, **42**(1), 1 (2018).
- [11] M.A. Green, K. Emery, Y. Hishikawa, W. Warta, E.D. Dunlop, D.H. Levi, and H. Baillie, Solar cell efficiency tables (version 49), *Prog. Photovolt: Res. Appl.* **25**(1), 3 (2017), <https://doi.org/10.1002/ppp.2855>
- [12] N. Khoshsirar, N.A. Yunus, M.N. Hamidon, S. Shafie, and N. Amin, *Optik*, **126**(7-8), 681 (2015). <https://doi.org/10.1016/j.ijleo.2015.02.037>
- [13] M. Mostefaoui, H. Mazari, S. Khelifi, A. Bouraiou, and R. Dabou, *Energy Procedia*, **74**, 736 (2015). <https://doi.org/10.1016/j.egpro.2015.07.809>
- [14] F. Za'abar, A.W. Zuhdi, M.S. Bahrudin, S.F. Abdullah, M.N. Harif, and A.H. Hasani, in: *2018 IEEE International Conference on Semiconductor Electronics (ICSE)*, (IEEE, Kuala Lumpur, Malaysia, 2018), pp. 209-213. <https://doi.org/10.1109/SMELEC.2018.8481289>
- [15] J. Park, and M. Shin, *Energies*, **11**(7), 1785 (2018). <https://doi.org/10.3390/en11071785>
- [16] M.B. Hosen, A.N. Bahar, M.K. Ali, and M. Asaduzzaman, *Data Brief*, **14**, 246 (2017). <https://doi.org/10.1016/j.dib.2017.07.054>
- [17] T. Shawky, M.H. Aly, and M. Fedawy, *IEEE Access*, **9**, 75283 (2021). <https://doi.org/10.1109/ACCESS.2021.3080391>
- [18] A. Sylla, S. Touré, and J.P. Vilcot, *Int. J. Sci. Res.* **6**(11), 855 (2017). <https://doi.org/10.4236/ampc.2011.13014>
- [19] K. Luo, Y. Sun, L. Zhou, F. Wang, and F. Wu, *Journal of Semiconductors*, **38**(8), 084006 (2018). <https://doi.org/10.1088/1674-4926/38/8/084006>
- [20] J. Park, and M. Shin, *Energies*, **11**(7), 1785 (2018). <https://doi.org/10.3390/en11071785>
- [21] H.I. Abdalmageed, M. Fedawy, and M.H. Aly, *Journal of Physics: Conference Series*, **2128**(1), 012009 (2021). <https://doi.org/10.1088/1742-6596/2128/1/012009>
- [22] S. Tobbeche, S. Kalache, M. Elbar, M.N. Kateb, and M.R. Serdouk, *Optical and Quantum Electronics*, **51**(8), 1 (2019). <https://doi.org/10.1007/s11082-019-2000-z>
- [23] SILVACO, Inc. ATLAS User's Manual device simulation software. 701 Patrick Henry Drive, Bldg. 2 March 20, (2012).
- [24] N. Khoshsirar, and N.A. Yunus, in: *2013 IEEE Conference on Sustainable Utilization and Development in Engineering and Technology (CSUDET)*, (IEEE, Selangor, Malaysia, 2013) pp. 63-67. <https://doi.org/10.1109/CSUDET.2013.6670987>
- [25] J.M. Olson, D.J. Friedman, S. Kurtz, *Handbook of Photovoltaic Science and Engineering*, West Sussex, first ed. (John Wiley and Sons, 2003), pp. 567-616. <https://doi.org/10.1002/0470014008>
- [26] J. Raymond, and I. Kilway. Thesis: Five- Junction Solar Cell Optimization Using Silvaco-Atlas, in: *Naval Postgraduate School*, (Monterey, California, 2017). <https://doi.org/NSN 7540-01- 280-5500>
- [27] SILVACO, solarex12, Thin Film Tandem Solar Cell, (2015). <https://doi.org/NSN 7540-01-280-5500>

ВПЛИВ БУФЕРНОГО ШАРУ ZnS НА ЕФЕКТИВНІСТЬ СОНЯЧНИХ ЕЛЕМЕНТІВ CIGS

Лайд Абделалі^а, Хамза Абід^а, Ікрам Зідані^а, Аїсса Мексі^б, Абделлах Бугенна^с, Заїд Бендауді^д^аЛабораторія прикладних матеріалів, Університет Джиллалі Ліабес Сіді-Бель-Аббес, Алжир^бВідділ електротехніки Університет наук і технологій Орану, Алжир В.Р 1505, Ель Мнауер, Оран, Алжир^сЛабораторія електротехніки Орана, Департамент електроніки, Факультет електротехніки, Університет наук і технологій Орана (MB-USTO), 31000, Оран, Алжир^дВідділ електротехніки та автоматики, Університет Релізану, Алжир

Тонкоплівкові сонячні елементи на основі Cu(In,Ga)Se₂ (CIGS) наразі є одними з найефективніших. Сульфід цинку (ZnS) є найкращим буферним шаром, який використовується в сонячних елементах на основі CIGS, оскільки він нетоксичний і має широку заборонену зону. У цьому дослідженні ми представляємо моделювання сонячної батареї CIGS з буферним шаром ZnS, виконане за допомогою симулятора Silvaco-Atlas. Ми досягли ефективності 24,13%, струму короткого замикання 37,81 мА/см², напруги холостого ходу 740 мВ і коефіцієнта заповнення 78,78% при ширині забороненої зони близько 1,41 еВ, що відповідає відношенню χ 0,5. Фотоелектричні характеристики сонячної батареї ZnS/CIGS покращуються шляхом оптимізації впливу параметрів шару, таких як товщина, щільність акцепторів і донорів поглинача CIGS і буферного шару ZnS. Для акцептора ZnS товщиною 0,035 мкм з щільністю 6×10^{17} см⁻³ і донора CIGS товщиною 3 мкм з щільністю 1018 см⁻³ максимальна ефективність покращилася до 27,22%.

Ключові слова: буферний шар (ZnS); CIGS; сонячна батарея; оптимізація; Silvaco-Atlas